Study of geometrical and electronic effects induced by hydrogen chemisorption on supported Pt particles. Analysis of Pt–H EXAFS and Pt–H anti-bonding state shape resonances

D.C. Koningsberger [a,*], M.K. Oudenhuijzen [a], J.H. Bitter [a] and D.E. Ramaker [b]

[a] *Department of Inorganic Chemistry and Catalysis, Debye Institute, Utrecht University, PO Box 80083, 3508 TB Utrecht, The Netherlands*
[b] *Department of Chemistry and Materials Science Institute, George Washington University, Washington, DC 20052, USA*

Geometrical and electronic effects induced by hydrogen chemisorption on supported Pt particles are studied by analysing the Pt–H anti-bonding shape resonance. The fundamental principles of a new analysis method of the L_2 and L_3 X-ray absorption edges are summarised. The method is used for studying the Pt–H bonding properties of weakly and strongly bonded hydrogen on surfaces of supported metal catalysts. Also the interaction of hydrogen with a Pt/CeO_2 catalyst as a function of the reduction temperature is investigated. The new analysis method makes it possible to follow the changes in the electronic structure of a Pt/Al_2O_3 catalyst as a function of the metal particle size.

Keywords: Pt–H EXAFS, Pt–H anti-bonding state shape resonance, hydrogen chemisorption, supported Pt catalysts, metal–support interaction

1. Introduction

Several studies in the literature have shown that hydrogen significantly affects the near-edge region of the Pt and Pd $L_{2,3}$ X-ray absorption edges. Mansour and Sayers [1] observed that the areas of the Pt $L_{2,3}$ white lines increased with exposure to H_2 in comparison to Pt foil and developed a quantitative technique for determination of the number of unoccupied d-electron states. Lytle et al. [2] observed significant changes in white line shape and intensity of the Pt $L_{2,3}$ edges for Pt/SiO_2 heated in H_2 vs. He and as a function of temperature. Samant and Boudart [3] noted similar changes in H–Pt vs. He/Pt clusters dispersed in Y zeolite. Vaarkamp et al. [4] showed an effect of interfacial hydrogen between the platinum cluster and the support on the Pt $L_{2,3}$ white line in an attempt to explain the difference in reactivity of γ-Al_2O_3-supported Pt particles as a function of reduction temperature. By comparing experimental data with multiple scattering calculations, Soldatov et al. [5] found that H introduced a multiple scattering state in the Pd L_3 white lines of $PdH_{0.6}$. Asakura et al. [6] and Reifsnyder et al. [7] suggested a new Pt–H resonance state visible in XAFS data after hydrogen adsorption on supported Pt particles. Finally, Boyanov et al. [8] observed two features in the H/Pt minus Pt foil $L_{2,3}$ difference spectra of Pt clusters supported on zeolite Y and interpreted them as spin–orbit doublets.

Recently, it has been shown by our groups [9,10] that chemisorption of hydrogen induces a Pt–H anti-bonding state shape resonance, which changes dramatically with the support. The resonance appears just above the Fermi level at the Pt L_3 edge (see also figure 1). A novel analysis method of the platinum L_3 and L_2 X-ray absorption edges of supported Pt/LTL catalysts [9] made it possible to isolate this anti-bonding state shape resonance. The difference in energy of this anti-bonding state (E_{res}) with respect to the Fermi level (E_F) is strongly affected by the charge compensating cations (H^+, K^+) in LTL zeolite: i.e., E_{res} decreases with increasing alkalinity [9,10]. This decrease in E_{res} can be directly correlated with the decrease of the neopentane hydrogenolysis turnover frequency (TOF) of Pt/LTL with increasing support alkalinity [11]. Similar results have been obtained for Pt particles dispersed inside Y zeolite [12], where the changes vary strongly with the support; i.e., 4.7 eV larger for Pt/H-USY than for Pt/NaY.

These results were attributed to a Coulomb interaction or field between the metal particles and interfacial support oxygen ions, which shifts the metal electron binding energies. As a result, the ionisation potential of the metal particles decreases with increasing negative charge on the support oxygen atoms. These results show that the potential

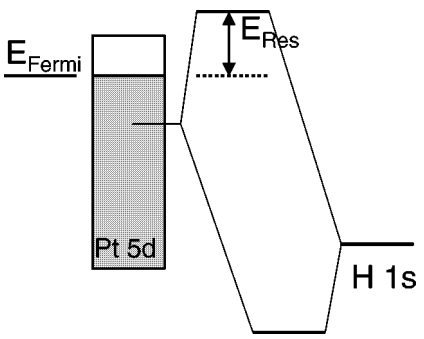

Figure 1. Molecular orbital (MO) picture showing formation of bonding and anti-bonding orbitals derived form a surface Pt orbital and the H 1s orbital (see also [16]).

* To whom correspondence should be addressed.

of the oxygen ions is not only a function of the alkalinity of the support, but also a function of the Si/Al ratio of the support and the polarisation field of the charge compensating cations (H^+, Na^+, La^{3+} and extra-framework Al).

The results, briefly summarised above for Pt/LTL and Pt/Y catalysts clearly reveal that the metal particles experience an electronic interaction that is determined by the properties of the support. These data further demonstrate that the change in the Pt electronic structure directly influences the catalytic properties of the catalyst. Moreover, the shifts in E_{res} directly correlate with the observed changes in the AXAFS data for the Pt/LTL and Pt/Y catalysts, as discussed in the preceding paper of this issue [11–13]. This work demonstrates that the Pt–H anti-bonding state shape resonance is an extremely valuable new tool to obtain information on the influence of the support on the electronic structure and catalysis of supported metal particles.

This new analysis method, when applied to the platinum L_3 and L_2 X-ray absorption edges of supported Pt catalysts, also shows the presence of Pt–H XAFS arising from direct scattering by hydrogen. The cross section for electron scattering from hydrogen falls off so strongly with energy that in the high energy range normally used for Fourier transformation in EXAFS analysis ($E \geqslant 25$ eV), the detection of hydrogen neighbours at the surface of the platinum particles is impossible. However, at energies close to the absorption edge (5–10 eV) the Pt–H XAFS is visible [9]. The analysis of the data obtained previously for a Pt/saponite catalyst illustrated that information can be obtained on the Pt–H bonding length at the surface of the supported Pt particles. Fitting the data, with the help of the Pt–H phase shift and backscattering amplitude calculated with the FEFF7 XAFS code gave good agreement with the data. These results show that geometrical information on hydrogen chemisorption can be obtained from an analysis of the Pt–H XAFS data.

In this paper, the fundamental principles of the new analysis method applied to the Pt L_2 and L_3 absorption edges will be summarised and then applied to hydrogen chemisorption. The new analysis procedure will be used first to obtain geometrical information concerning the Pt–H bonding on a Pt/K–Al_2O_3 catalyst. It will be demonstrated that the Pt–H XAFS changes as expected for weakly and strongly adsorbed hydrogen. This gives detailed information on the nature of this weakly adsorbed hydrogen. Further, the interaction of hydrogen with Pt/CeO_2 is studied as a function of the reduction temperature. The results will show that the interaction of hydrogen with the surface of the platinum particles changes as the catalysts is reduced at high temperature due to the appearance of the SMSI state.

The new analysis method will further be applied to obtain electronic structure information. The Pt–H anti-bonding state shape resonance for an acidic Pt/Cl–Al_2O_3 catalyst is analysed. These data will be combined with those obtained from earlier studies to demonstrate that the background phase (Φ) is a function of E_{res} confirming the expected behaviour of a shape resonance. A new procedure will be introduced to generate the functional for the background phase. The behaviour of E_{res} for the Pt/Cl–γ-Al_2O_3 is in line with the data previously obtained for Pt/LTL and Pt/Y: i.e., E_{res} decreases with increasing negative charge on the support oxygen ions. Moreover, the data now available for Pt on acidic supports show that, as expected, E_{res} decreases with increasing particle size, showing a decrease in the effect of the support for larger particles.

2. Experimental

2.1. Catalyst preparation

The preparation of the Pt/LTL, Pt/Sap6 and the Pt/Y catalysts is described in [9,11], respectively. The CeO_2 support (130 m^2/g, 99.9% pure) was heated to 823 K in H_2 and held there for 4 h. Subsequently the support was reoxidised at 773 K in 5% O_2/He. The resulting support has a surface area of 80 m^2/g. This support was impregnated with $[Pt(NH_3)_4](NO_3)_2$, dried at 373 K, reduced at 573 K in H_2 and stored for further use after passivation at RT. The Al_2O_3 support (alumina sol, Criterion) was calcined at 723 K to produce pseudo boehmite. Alkaline alumina (0.25 wt%) was prepared by adding of KOH and recalcination at 273 K. This support was impregnated with $[Pt(NH_3)_4](NO_3)_2$ (2 wt% Pt), dried, reduced in H_2 at 623 K and stored for further use (catalysts denoted by Pt/K–Al_2O_3). The pseudo boehmite was also impregnated with a solution of H_2PtCl_6 (2 wt% Pt), dried, calcined at different temperatures and further reduced at 623 K. Two samples with different averaged particle sizes were used in this study: these are denoted as Pt/Cl–Al_2O_3 (I) and (II).

2.2. XAFS data collection

The X-ray absorption spectra at the Pt L_3 and L_2 edges were taken at the SRS (Daresbury, UK) Wiggler Station 9.2, using a Si(220) double crystal monochromator. The monochromator was detuned to 50% maximum intensity to avoid higher harmonics present in the X-ray beam. Experiments were also performed at the ESRF (Grenoble, France) at BM29, using a Si(311) crystal. All experiments were carried out in transmission mode. The monochromator was detuned to 70% of maximum intensity. XAFS data were also collected at HASYLAB synchrotron at beamline X1.1. (Hamburg, Germany) in transmission mode. The monochromator was detuned to 50% of maximum intensity. All measurements were done in transmission mode using ion chambers filled with Ar to have an X-ray absorbency of 20% in the first and of 80% in the second ion chamber.

Samples were pressed into self-supporting wafers (calculated to have an absorbency of 2.5) and placed in a controlled atmosphere cell [14]. Spectra were recorded at liquid-nitrogen temperature after reduction in H_2 (samples

further denoted by H–Pt) and subsequently treated in helium (Pt/LTL, Pt/CeO_2) or vacuum (all other samples) to remove chemisorbed hydrogen (samples further denoted by Pt).

2.3. XAFS data analysis

The final XAFS spectrum was obtained by averaging three to four scans. The pre-edge background was approximated by a modified Victoreen curve [4], and the background was subtracted using cubic spline routines [15]. Spectra were normalised by dividing the absorption intensity by the height of the absorption edge at 50 eV above the edge [4].

3. Isolation of the Pt–H anti-bonding state shape resonance and Pt–H EXAFS

3.1. Pt–H anti-bonding state shape resonance

Hydrogen chemisorption induces a bonding and an anti-bonding orbital as reported by Hammer et al. [16] (see figure 1). The partially occupied "dangling" platinum surface orbitals form a bond with the hydrogen 1s orbital producing the bonding and antibonding Pt–H orbitals. The anti-bonding state can be viewed as a localised state degenerate with a continuum state; the latter described by the Pt–H EXAFS final state wave function. The outgoing photoelectron, when excited into the antibonding orbital will reside temporarily in the potential well determined by the AS state. Subsequently, this electron will escape into the continuum becoming a resonance with the Pt–H XAFS final state wave function. This one electron process is termed a "shape" resonance and exhibits the well-known Fano-like resonance profile. Its effect on the scattering cross section $\sigma(E)$ can be related to an EXAFS function $\chi(E)$ via the normal expression $\sigma(E) = \mu(E)(1 + \chi(E))$. It can be shown [9] that

$$\chi(E) = (1/k)A \sin\Phi\big[(1 - q\varepsilon)/\big(1 + \varepsilon^2\big)\big], \qquad (1)$$

with A an amplitude factor, $q = \cot\Phi$ and $\varepsilon = (E - E_{\text{res}})/\Gamma$. Φ is denoted as the background phase and is determined by the total phase found in EXAFS: $\Phi = 2kR + \phi$, with ϕ the phase determined by the absorber (Pt) and backscatterer (H). ε is the normalised energy scale relative to the resonance energy (E_{res}), whereby Γ represents the resonance width. A fit to the experimentally observed AS lineshape gives values for E_{res}, Γ, A and Φ. E_{res} is defined as the difference in energy between the Fermi level (E_{F}) and the anti-bonding state (AS)

The position in energy of the anti-bonding state (E_{res}) relative to the Fermi level determines the resonance properties with the Pt–H final state wave function. The phase of the shape resonance is therefore directly determined by E_{res}. By taking k and A equal to 1 in equation (1), the following expression can be obtained for the shape resonance:

$$\chi(\varepsilon) = \sin\Phi\big[1/\big(1 + \varepsilon^2\big)\big] - \cos\Phi\big[\varepsilon/\big(1 + \varepsilon^2\big)\big]. \qquad (2)$$

In each panel of figure 2 $\chi(\varepsilon)$ is plotted as a function of ε with the phase Φ as a parameter. Figure 2 shows how the shape of the resonance changes for different values of Φ. This figure makes clear how the shape of the Pt–H anti-bonding state shape resonance is determined by Φ and consequently by the position in energy of the anti-bonding state.

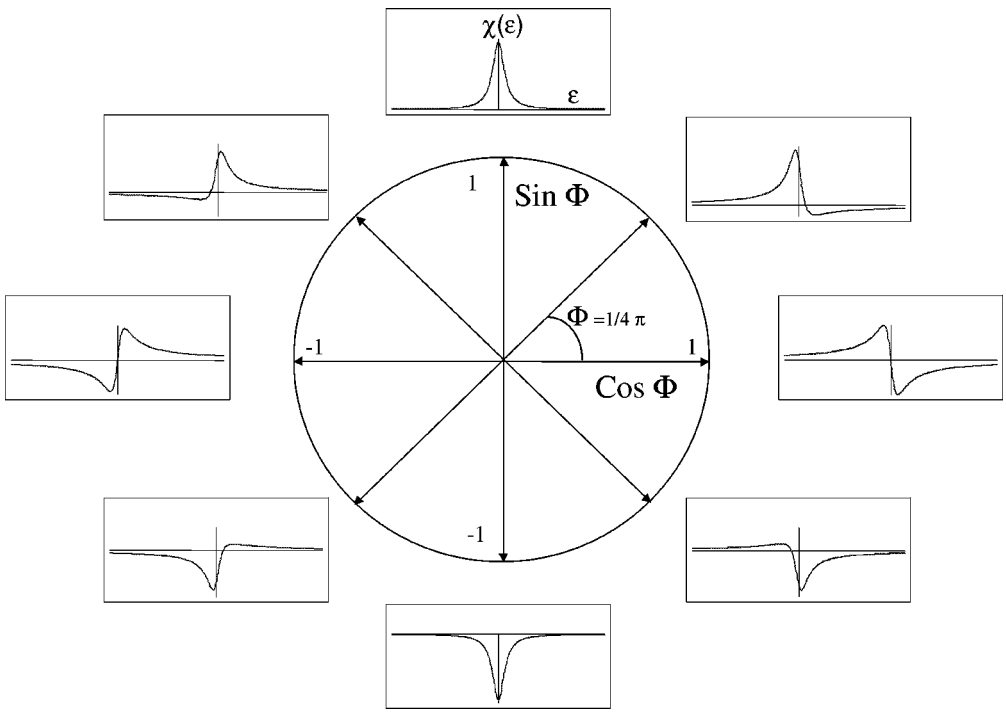

Figure 2. The shape of the anti-bonding shape resonance (AS) as a function of energy (E) for different values of the background phase (Φ).

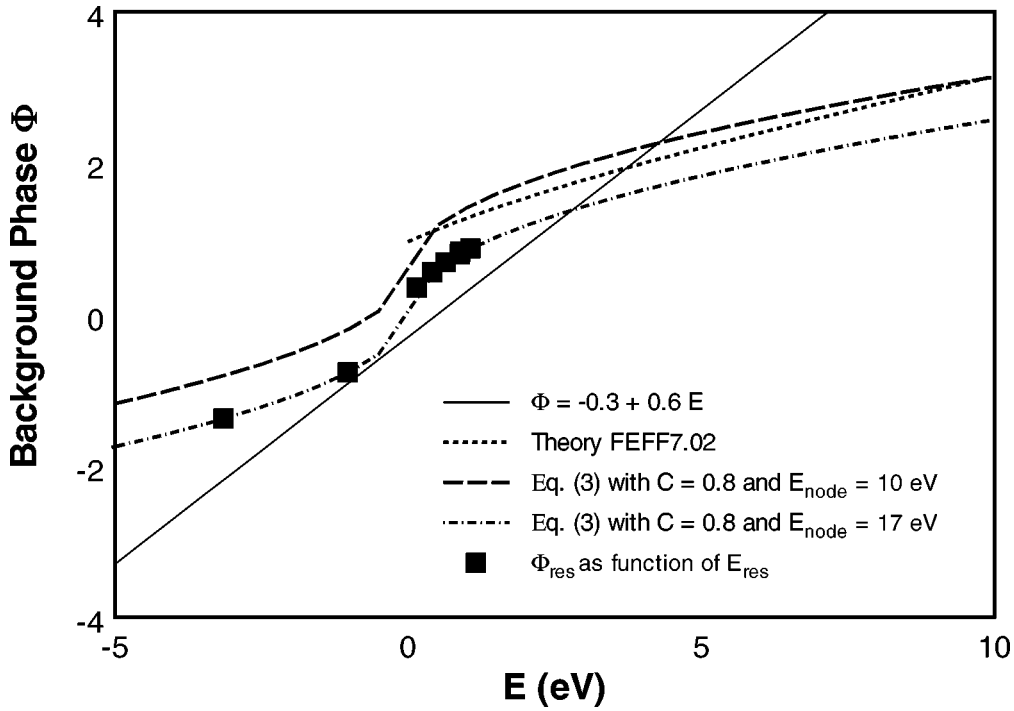

Figure 3. Background phase Φ as a function of E: (——) approximated by $\Phi = -0.3 + 0.6E$ (used in [10,12]); (· · ·) calculated from FEFF7.02 for a Pt–H EXAFS with Pt–H distance of 1.9 Å; (- - -) calculated with equation (3) using $C = 0.8$ and $E_{\text{node}} = 10$ eV; (-·-·-) calculated with equation (3) using $E_{\text{node}} = 17$ eV and optimised fit values $C = 0.8$ for fitting Pt–H anti-bonding state of catalysts samples (see table 5); (■) values of Φ_{res} as a function of E_{res} as obtained from the fitting of the data to equation (1), as described in the text.

3.2. Determination of the EXAFS background phase Φ

In our previous work, the background phase was related to E_{res} by taking $\Phi = \alpha + \beta|E_{\text{res}}|$ with the optimal values found to be $\alpha = -0.3$ and $\beta = 0.6$. The phase Φ is plotted against E in figure 3 with a solid line. A more accurate description of the phase Φ is obtained by using the normal expression for the EXAFS phase: $\Phi = 2kR + \phi$. In a small interval of k it is reasonable to use $\phi = a + bk$, which gives $\Phi = k(2R + b) + a$. Here the constant a can be eliminated by observing that Φ must be π when the normal EXAFS (proportional to $\sin\Phi$) has a true node with negative slope. We use this second node, because the first node can be affected by the position of the edge, and therefore its position is not only dependent on Φ. If this second node is denoted as k_{node}, then we have $\Phi = (2R + b)(k - k_{\text{node}}) + \pi$ in the vicinity of k_{node}. This can be expressed on the energy scale:

$$\Phi = C\left(\sqrt{|E|} - \sqrt{E_{\text{node}}}\right) + \pi \qquad (3)$$

with $C = 0.51(2R + b)$ taking $k = 0.51\sqrt{|E|}$. Negative energies relative to the edge (i.e., below the Fermi level) must be allowed since the shape resonance is observed in the XAS final state in the presence of the core hole. The Pt–H anti-bonding orbital is more localised than the itinerant d-orbitals. This shifts the resonance to higher binding energies due to the core-hole electron attraction, and this shift will be much larger than for the itinerant d-orbitals and Fermi level. This means that some AS states, i.e., those close to the Fermi level in the ground state, can have negative values for E_{res} (i.e., appear below the Fermi level or edge) in the final state. It is assumed here that the constant C is the same immediately above and below the Fermi level.

Equation (3) shows that the total phase Φ is not linear but varies as the square root of the photon energy E. Expression (3) was used previously for analysing the AS resonances resulting from the Pt–O interactions on the surface of Pt particles in a fuel cell [17]. In that instance E_{res} had values ranging from -8 to 3 eV, a sufficiently large range to make the simple linear expression inappropriate. Thus we utilise the more accurate expression here as well.

A Pt–H EXAFS function was calculated with FEFF7.02 using a Pt–H bond distance of 1.9 Å and the Dirac–Hara potential, which we have found previously to give the best representation for Pt–H scattering. The calculated total phase Φ as calculated from FEFF7.02 is plotted in figure 3 with a dotted line. FEFF7.02 cannot generate phase shifts at negative energies and the accuracy of E_0 can be questioned. Therefore, equation (3) is used to approximate Φ for negative values of E. An examination of the calculated ϕ vs. k from FEFF7.02 reveals that in the range from $k = 0$ ($E = 0$ eV) to 2 ($E = 15.2$ eV), b is determined to be -2.2. This gives for $C = 0.51(2R+b)$ a value of 0.8. The second node was found at 10 eV for the Pt–H EXAFS as calculated with FEFF7.02. Φ was then calculated from -5 to 10 eV (see figure 3 long dashed line) using equation (3) with $b = 0.8$ and $E_{\text{node}} = 10.0$. It can be seen in figure 3 that expression (3) can be made to approximate, particularly at higher energies, the Φ calculated from FEFF7.02.

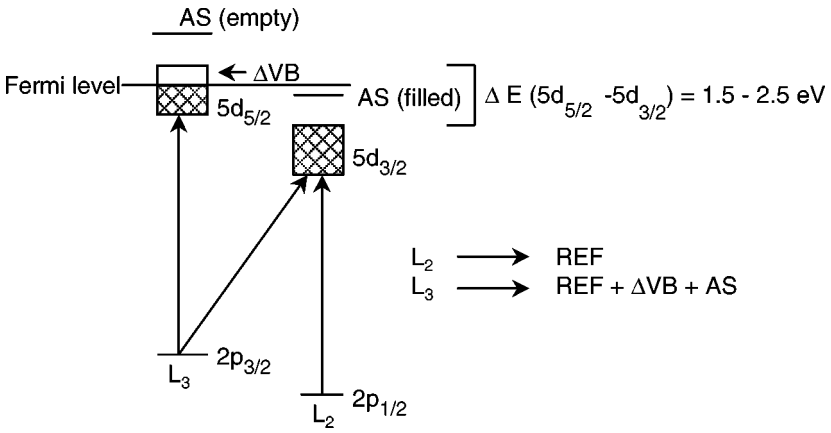

Figure 4. Illustration of spin-orbital coupling effects in the X-ray absorption $L_{2/3}$ edge spectra and 5d valence band. REF: L_2 edge used as reference, AS: Pt–H anti-bonding state, ΔVB: empty valence d-orbitals. The energy levels (2p and 5d) do not have the same scale! Figure taken from [12].

3.3. Explanation of the method

As illustrated in figure 4, the spin–orbit interaction in both the core and valence levels introduces large differences between the L_3 ($2p_{3/2} \rightarrow 5d_{5/2}$, $5d_{3/2}$) and L_2 ($2p_{1/2} \rightarrow 5d_{3/2}$) white lines, both in shape and intensity (the $2p_{3/2}$–$2p_{1/2}$ splitting is around 1709 eV, and the $5d_{5/2}$–$5d_{3/2}$ splitting around is 1.5–2.5 eV) [18]. The L_3 edge reflects the empty valence band levels (ΔVB) of both the $d_{5/2}$ and $d_{3/2}$ bands, weighted as $d_{5/2}/d_{3/2} = 6$, however, the L_2 edge reflects only the $d_{3/2}$ level [18]. For small platinum clusters, the $5d_{3/2}$ is believed to be completely filled due to band narrowing relative to platinum bulk, therefore, it is assumed that there is no Pt d valence band (ΔVB) contribution to the L_2 white line (see further discussion [9]). Table 1 summarises the important contributions that will be visible in the four X-ray absorption edges of platinum in Pt/LTL catalysts, based on the assumptions and theory described in [9]. The L_2 edge spectrum for "clean" Pt clusters can be used as the reference (REF), since this spectrum arises from the "free" atom absorption and the EXAFS contributions. The L_3 spectrum of the clean Pt cluster contains in addition the electronic (empty valence band: ΔVB) contribution [9]. The L_2 spectrum for the H–Pt sample is different from the REF spectrum, because of changes in geometry of the cluster induced by chemisorption of hydrogen. As shown in [9], these changes in geometry (ΔXAFS) of the cluster include changes in the Pt–Pt co-ordination due to adsorption of hydrogen as well as the presence of Pt–H EXAFS. The Pt–H bonding orbital is primarily localised on the H atom, and the anti-bonding state (AS) is localised more on the surface Pt atoms, causing the $5d_{3/2}$ component of the AS state to shift upward. Therefore, the excitation of the outgoing electron to the empty antibonding orbital should be evident only in the near edge spectrum of the H–Pt L_3 X-ray absorption edge. Finally, the L_3 spectrum for the H–Pt sample contains both the geometric (ΔXAFS) and electronic (ΔVB + AS) changes from the reference.

Subtracting the different edges from each other isolates the different contributions: ΔVB, ΔXAFS, AS. Before the different contributions can be separated from the X-ray absorption spectra, the edges have to be aligned in order to account for initial and final state effects. This alignment procedure is extensively discussed in [9].

Table 1
Main information present in the Pt L_3 and L_2 near edge spectra.

Sample	Edge	
	L_3	L_2
H–Pt	REF + ΔXAFS + ΔVB + AS	REF + ΔXAFS
Pt	REF + ΔVB	REF

Table 2
Fit results for the Pt–Pt coordination of Pt/K–Al_2O_3 samples.[a]

Treatments	N	R (Å)
Red400	6.5	2.75
Vac50	6.5	2.71
Vac200	6.7	2.68

[a] All fits were done in R-space, k^2 weighting, with 1.6 Å $< R <$ 3.2 Å and 2.5 Å$^{-1} < k <$ 14.0 Å^{-1}.

4. Results

4.1. Pt–H EXAFS, strongly and weakly adsorbed hydrogen on Pt/K–γ-Al_2O_3

XAFS data were collected after reduction at 400 °C (Red400), after evacuation at 50 °C (Vac50) and subsequent evacuation at 200 °C (Vac200). A summary of the Pt–Pt coordination parameters (coordination numbers and distances) obtained from the EXAFS data analysis is given in table 2. A full discussion of the EXAFS data is given in [19]. The L_2 edge data collected after the different treatments are displayed in figure 5. It can be seen that the height of the L_2 edge continuously decreases in the order Red400, Vac50 and Vac200 due to the desorption of hydrogen. The data measured after reduction at 400 °C contain both weakly and strongly adsorbed hydrogen. Evacuation at 50 °C removes the weakly adsorbed hydrogen,

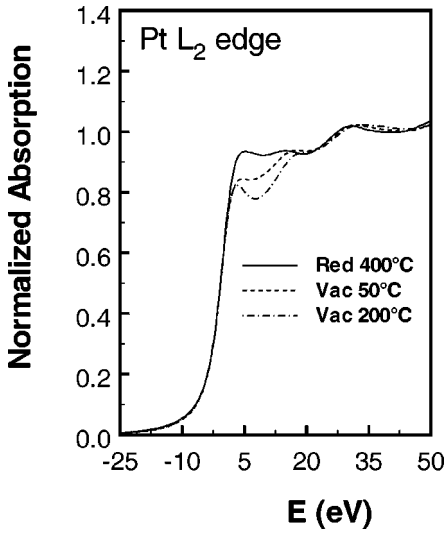

Figure 5. L_2 edges of Pt/K–Al_2O_3 after reduction at 400 °C (——), after evacuation at 50 °C (- - -) and subsequent evacuation at 200 °C (-·-·-). Data taken from [19].

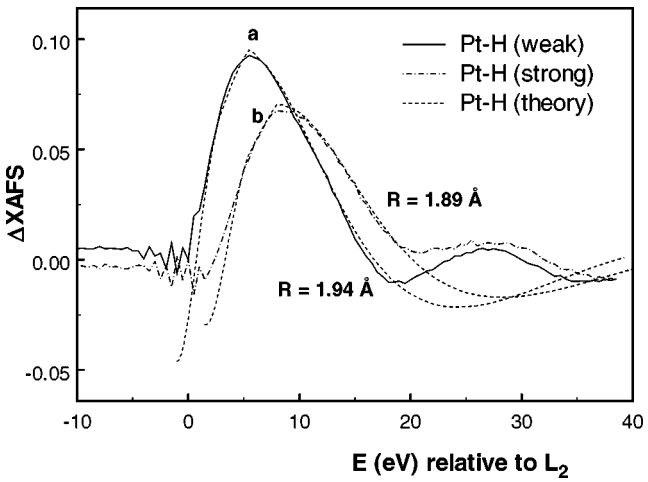

Figure 6. Isolated Pt–H EXAFS and fits (- - -) for weakly and strongly adsorbed hydrogen on Pt/K–Al_2O_3. (a) L_2(Red400) – L_2(Vac50) (weakly adsorbed hydrogen) (——). Fit with Pt–H bond distance of 1.94 Å. (b) L_2(Vac50) – L_2(Vac200) (strongly adsorbed hydrogen) (-·-·-). Fit with Pt–H bond distance of 1.89 Å. Data taken from [19].

whereas subsequent evacuation at 200 °C leads to the disappearance of the strongly bonded hydrogen. By taking the Vac50 data as a reference for the Red400 data, the difference L_2(Red400) – L_2(Vac50) produces the ΔXAFS function, which in this case gives the Pt–H EXAFS of the weakly bonded hydrogen. The ΔXAFS function is plotted in figure 6(a), solid line. The ΔXAFS function of the strongly bonded hydrogen can be obtained by using the Vac200 data as the reference for the Vac50 experiments. The difference L_2(Vac50) – L_2(Vac200) gives the ΔXAFS function of the strongly bonded hydrogen (see figure 6(b), dashed–dotted line). Using the FEFF7.02 code, the ΔXAFS functions can be fitted with a Pt–H coordination with a distance of 1.94 and 1.89 Å, respectively. These fits are shown in figure 6 (a) and (b) with the dotted lines.

Table 3
Fit results for the Pt–Pt coordination of Pt/CeO_2 samples.[a]

Treatment	N	R (Å)
Red200	10.2	2.77
He200	10.0	2.76
Red500	9.8	2.76
He500	7.7	2.77

[a] All fits were done in R-space, k^2 weighting, with 1.6 Å $< R <$ 3.1 Å and 2.5 Å^{-1} $< k <$ 14.0 Å^{-1}.

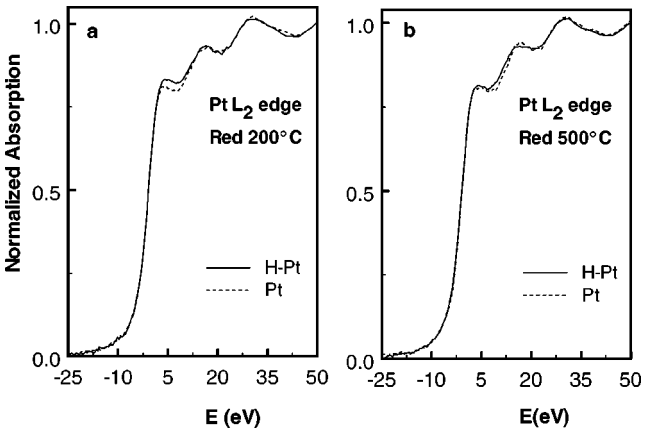

Figure 7. L_2 edge of Pt/CeO_2: (a) after reduction at 200 °C (——) and evacuation at 200 °C (- - -); (b) after reduction at 500 °C (——) and evacuation at 500 °C (- - -). Data taken from [20].

4.2. Pt–H EXAFS, normal and SMSI state of Pt/CeO_2

A summary of the coordination parameters (Pt–Pt coordination numbers and distances) obtained from the analysis of the EXAFS data measured after low and high-temperature reduction and evacuation are given in table 3. The EXAFS data-analysis and results are fully discussed in [20]. The L_2 edges of the XAS data of the Pt/CeO_2 sample after reduction at 200 °C (H–Pt) and evacuation at 200 °C (Pt) are plotted in figure 7(a). The desorption of hydrogen leads to a decrease in the L_2 edge intensity. Figure 7(b) gives the L_2 edges obtained after reduction at 500 °C (SMSI state) (H–Pt) and the L_2 edge after evacuation at 500 °C (Pt). The differences between the H–Pt and Pt edges in the normal and SMSI state are not the same as can be seen more clearly in figure 8 (a) and (b) by comparing the ΔXAFS functions obtained by taking the difference L_2(H–Pt) – L_2(Pt). Two maxima can be observed in the ΔXAFS data of the SMSI state. Fitting the ΔXAFS data obtained after reduction at 200 °C with the help of the FEFF7.02 code, resulted in a Pt–H coordination with a distance of 1.9 Å. The ΔXAFS data representing the SMSI state could not be fitted with a single Pt–H coordination. Including an additional coordination with molecular hydrogen (H_2) made it possible to reproduce the two maxima in the ΔXAFS data.

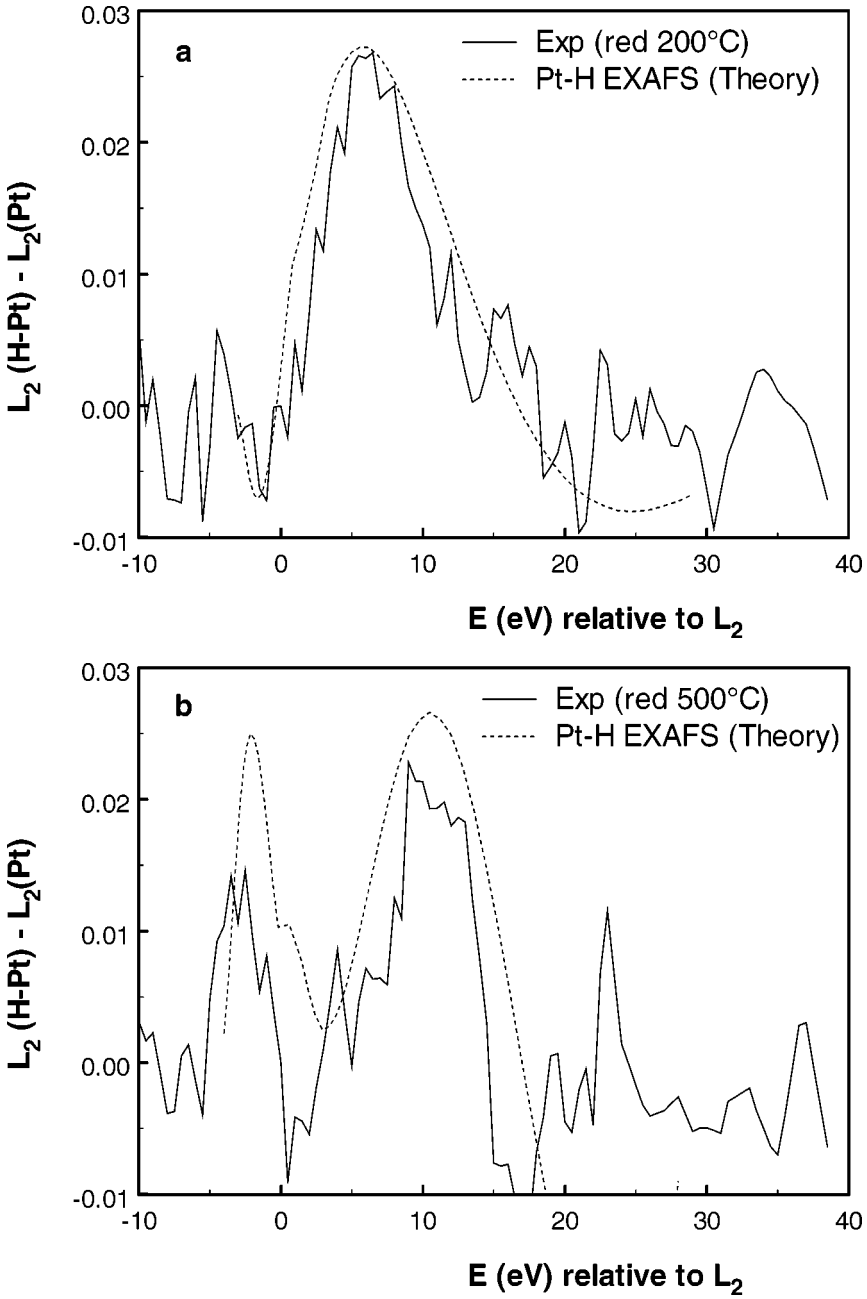

Figure 8. Isolated Pt–H EXAFS (——) and fits (- - -) of Pt/CeO_2. (a) L_2(H–Pt) − L_2(Pt) after reduction at 200 °C, representing normal chemisorbed hydrogen. Fit with single scattering Pt–H bond with distance of 1.9 Å. (b) L_2(H–Pt) − L_2(Pt) after reduction at 500 °C, representing the SMSI state. Fit with single scattering Pt–H bond with distance of 1.9 Å and linear Pt–H–H co-ordination with first H atom at 2.2 Å and second H atom at 2.9 Å including multiple scattering. Data taken from [20].

4.3. Isolation of the Pt–H anti-bonding state shape resonance of Pt/Cl–Al_2O_3

The EXAFS analysis of the two Pt/Cl samples reveals two different particle sizes. A summary of the EXAFS results is presented in table 4. Figure 9 displays the Pt L_2 and L_3 X-ray absorption edges for H–Pt/Cl–Al_2O_3 (I) (solid line) and Pt/Cl–Al_2O_3 (I) (dotted line) after the alignment procedure, as described in [9]. It can be seen that the presence of hydrogen chemisorption induces large changes in shape, intensity and position of the white lines of both

Table 4
Fit results for the Pt–Pt coordination of Pt/Cl–Al_2O_3 samples.[a]

Treatment	N	R (Å)
(I) Red400	6.6	2.73
(I) Vac200	6.1	2.68
(II) Red400	7.6	2.75
(II) Vac200	7.1	2.69

[a] All fits were done in R-space, k^2 weighting, with 1.6 Å $< R <$ 3.2 Å and 2.5 $Å^{-1} < k <$ 14.0 $Å^{-1}$.

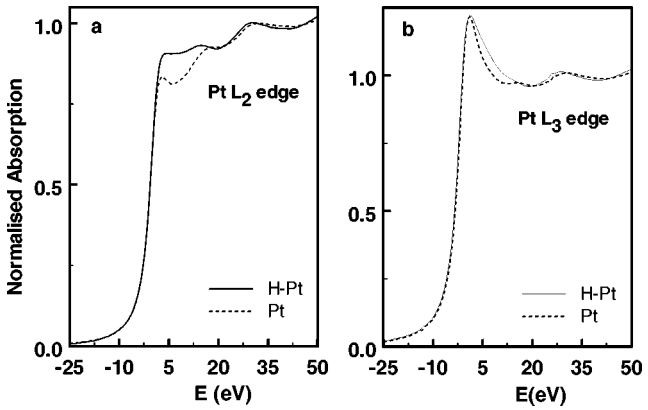

Figure 9. L_3 and L_2 edges of Pt/Cl–Al_2O_3 (I). (——) chemisorbed hydrogen (H–Pt) and (- - -) vacuum treatment at 200 °C (Pt).

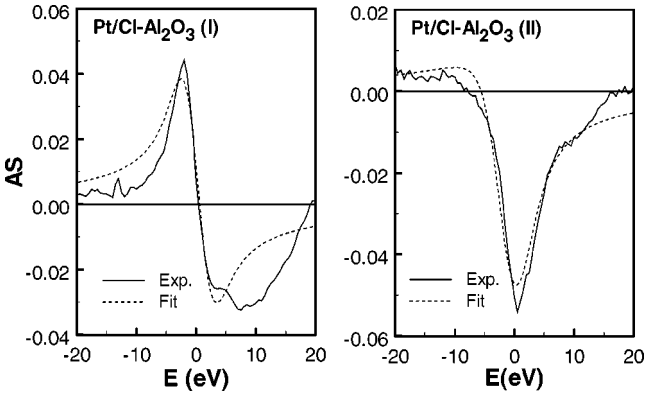

Figure 10. Pt–H anti-bonding shape resonance (AS) for Pt/Cl–Al_2O_3 (I) and (II) (——) and best fits (- - -) using equation (1).

edges, as previously observed [1–4]. The Pt–H anti-bonding state shape resonance (AS) can now be isolated by subtracting $\Delta L_2 = L_2$(H–Pt) $- L_2$(Pt) from $\Delta L_3 = L_3$(H–Pt) $- L_3$(Pt) (see also table 1). Figure 10 shows this antibonding resonance (solid lines) for each Pt/Cl–Al_2O_3 sample, and reveals that the lineshapes are different. The difference in lineshape can now easily be explained by figure 2. Since the support of both catalysts is the same, only the particle sizes are different, it can be concluded from figure 10 that the Pt–H AS shape resonance is a strong function of particle size due to the fact that the influence of the support is larger for smaller metal particles.

4.4. Optimisation of fit procedure to AS for Pt/LTL, Pt/Y and Pt/Cl–Al_2O_3 catalysts

Equation (1) was fitted to several experimental AS line shapes in a non-linear least squares fit procedure. A Gaussian broadening of 5 eV was added to account for the experimental resolution and core-hole lifetime broadening. The fit procedure was carried out using the expression given in equation (3) for the background Φ with the optimised values for C and $E_{\text{node}} = 17$ eV, as obtained from the position of the second node in the ΔXAFS data as described above. The experimental line shapes of AS found previously (Pt/LTL and Pt/Sap6 [9,10], Pt/Y [12]) together with the AS found for the two Pt/Cl–Al_2O_3 samples in this work were then fitted with three parameters for each resonance, i.e., E_{res}, Γ and A. The results are given in table 5. The AS and the corresponding fits are displayed in figure 11(a) for the acidic Pt/LTL (Si/Al = 0.63) and basic Pt/LTL (Si/Al = 1.25) samples. The results obtained for Pt/H-USY and Pt/NaY are shown in figure 11(b). As can

Table 5
Fit parameters obtained from non-linear least squares fit of Fano profile to the hydrogen induced shape resonance in experimental spectra: equation (3) using $C = 0.8$ and $E_{\text{node}} = 17$ eV was utilised to calculate Φ.[a]

Catalyst	A ($\pm$0.03)[c]	E_{res} (eV)[b] ($\pm$0.3)	Width Γ (eV) ($\pm$0.4)	Φ (calculated) ($\pm$0.1)
Pt/Cl–Al_2O_3 (I)	0.11	0.2	2.4	0.2
Pt/Cl–Al_2O_3 (II)	0.07	−1.0	4.8	−1.0
Pt/Na-Y	1.71	−3.1	0.6	−1.6
Pt/H-USY	1.58	0.9	0.6	0.6
Pt/Sap6	0.55	0.9	0.3	0.6
Pt/LTL (0.63)	0.60	1.1	0.6	0.7
Pt/LTL (0.96)	0.17	0.4	0.5	0.4
Pt/LTL (1.25)	0.26	−1.6	0.8	−1.1

[a] Applied experimental width: Gaussian, 5 eV.
[b] Relative to the L_2 absorption edge.
[c] Estimated uncertainty in each case.

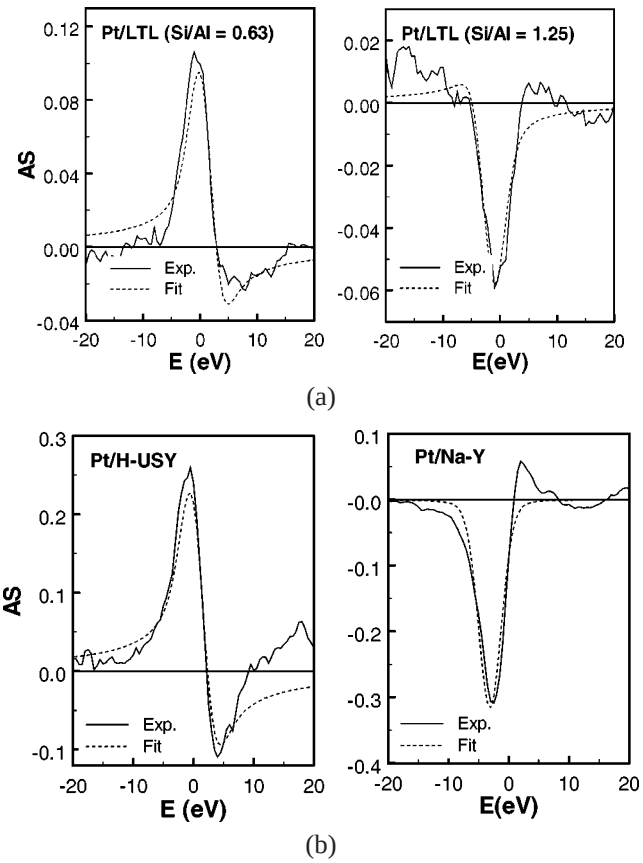

Figure 11. Pt–H anti-bonding shape resonance (AS) (——) and best fits (- - -) using equation (1): (a) Pt/LTL (0.63) and Pt/LTL (1.25); (b) Pt/H-USY and Pt/NaY.

be seen in figure 11 and as previously discussed in [10–12], the support has a strong influence on the electronic structure of the supported Pt particles.

5. Discussion

5.1. Pt–H EXAFS, strongly and weakly adsorbed hydrogen on Pt/K–Al_2O_3

It is well known from hydrogen chemisorption experiments that two types of adsorbed hydrogen can be distinguished. Evacuation at RT of a reduced catalyst, which is fully covered with adsorbed hydrogen, leads to desorption of weakly bonded hydrogen. Hydrogen uptake is measured after re-admission of hydrogen. The strongly chemisorbed hydrogen can be removed only after evacuation at high temperature (200 °C). The nature of this weakly adsorbed hydrogen is still not known; namely is it physisorbed or chemisorbed hydrogen? In a forthcoming paper [19], we will show that for both types of hydrogen a Pt–H anti-bonding state shape resonance can be observed. This implies that the weakly adsorbed hydrogen is indeed chemisorbed and not physisorbed. However, the value of E_{res} of the weakly chemisorbed hydrogen is smaller, which directly points to a weaker bond.

The results presented in figure 5 clearly show that the ΔXAFS function indeed describes a Pt–H XAFS. The smaller coordination distance for the Pt–H XAFS found by taking the difference L_2(Vac50) – L_2(Vac200) is in full agreement with that of strongly chemisorbed hydrogen. Moreover, it will be shown elsewhere [19] that the difference in amplitude of the Pt–H EXAFS functions correlates with the amounts of weakly and strongly bonded hydrogen as found in hydrogen chemisorption experiments. These data are the first to show that the analysis of the Pt–H EXAFS provides useful and detailed information about the different types of hydrogen chemisorption on supported Pt metal particles. Moreover, the detected Pt–H bond distances correlate nicely with the Pt–H bond strength as derived from hydrogen chemisorption experiments. The differences between the ΔXAFS functions and the fits at energies higher than 20 eV can be due to small changes in the Pt–Pt coordination as a function of the evacuation treatments. It is also possible that other Pt–H geometries have to be included in order to describe the differences found at energies higher than 20 eV. More research is needed to solve this problem.

5.2. Pt–H EXAFS, normal and SMSI state of Pt/CeO_2

In the literature, two models have been presented to describe the SMSI behaviour of metal particles dispersed onto supports, which are reducable at high temperature. Based upon TEM experiments, one model ascribes the loss of hydrogen chemisorption capacity after high-temperature reduction to physical blockage of the surface by support suboxide formation on the surface of the metal particles [21]. However, other experiments have been described in the literature, which demonstrate SMSI behaviour without observing any physical blockage of the surface. Based upon these experiments, another model has been put forward in which the SMSI state is described to arise from a change in electronic properties of the metal particles induced by the reduced support [22]. No detailed mechanism has been given yet to explain the origin of the induced changes in electronic structure of these metal particles.

In a forthcoming paper [20], we will show that after reduction at 500 °C of the Pt/CeO_2 catalysts, the hydrogen chemisorption capacity decreases to a large extent, but no physical blockage of the surface can be detected with HRTEM. The preliminary results presented here show that after reduction at 200 °C, a normal Pt–H XAFS can be observed with a bond length of 1.9 Å. In the SMSI state the data could be fitted with a Pt–H EXAFS with bondlength of 1.9 Å and a physisorbed molecular hydrogen (Pt–H_2). However, the signal to noise ratio in the Pt–H data shown in figure 8(b) does not allow us to draw positive conclusions about the 1.9 Å bondlength. It can also not be excluded yet that a Pt–H coordination other than Pt–H_2 could be present, such as H in a Pt three-fold hollow site. Better data and more detailed theoretical calculations are needed to put forward a definite geometrical model. However, it will be shown in [20] that the Pt–H anti-bonding state shape resonance (AS) shifts to lower energy after high-temperature reduction. This would directly imply a weaker Pt–H bond. Further increase of the SMSI state should lead to a further shift toward the Fermi level. This will increase the electron density in the anti-bonding state, which ultimately leads to the absence of any bonded hydrogen or chemisorption. The mechanism that causes the resonance shift in the SMSI state will be described in [20].

5.3. Pt–H anti-bonding state shape resonance

The use of expression (3) for the background phase Φ leads to slightly different values for E_{res} from that obtained previously for the Pt/LTL [10] and Pt/Y [12] catalysts. Expression (3) is believed to describe the background phase more accurately. However, the trends as observed previously for the influence of the support on the relative positions of E_{res} are still the same. The values obtained for E_{res} are plotted onto the curve derived for the background phase in figure 3.

5.4. Metal–support interaction

A relationship exists between the catalytic activity and the position of the H-induced shape resonance as a function of support properties as already shown in [10–12]. The electron charge on the support oxygen ions is affected by charge compensating cations (H^+, K^+) in LTL zeolite [10,11] and by the Si/Al ratio and the polarisation field of charge compensating cations (H^+, Na^+, La^{3+}) in Y zeolite [12]. The AXAFS data of the Pt/LTL [11] and Pt/Y [12]

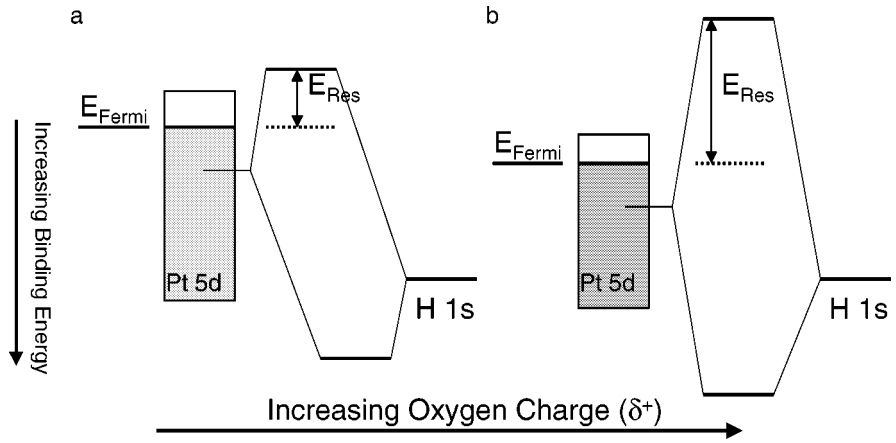

Figure 12. Molecular orbital (MO) picture showing formation of bonding and anti-bonding orbitals derived form a surface Pt orbital and the H 1s orbital: (a) neutral oxygen (see also [16]) and (b) positive charge on oxygen. Interacting d-orbitals are shifted to higher binding energy and E_{res} is larger (figure taken from [12]).

catalysts reveal that the support oxygen charge influences the Coulomb interaction between the platinum metal particles and the support (see preceding paper in this issue). The ionisation potential of the metal particle valence orbitals is found to increase with decreasing (more positive) electron charge on the support oxygen atoms. In accordance with this change, the Pt–H resonance data show that the resonance energy shifts to higher energy with decreasing (more positive) electron charge on the support oxygen ions (see also table 5).

This influence of the support on the AXAFS and E_{res} data of supported metal particles can be visualised in figure 12. The energy of the H 1s orbital is lower than the energy of the Pt valence orbitals [16] and does not change with catalyst composition. The difference in energy between the interacting H 1s and Pt 5d orbital decreases with increasing oxygen charge (more positive) on the support oxygen ions (as revealed in in the experimental AXAFS results). This would imply, that if nothing else changed, E_{res} should decrease; however, the experimental shape resonance results shows that E_{res} increases. This indicates that the covalent overlap in the Pt–H bond apparently increases with increasing oxygen charge (more positive) leading to a stronger Pt–H bond. The implication from the shape resonance analysis is that the position in energy of the Pt valence d-orbitals is influenced by the support thereby affecting the chemisorption energy of the adsorbate and consequently changing the catalytic behaviour of the metal particles. This is consistent with recently reported hydrogen TPD experiments, which show that the two peak positions around 90 and 100 °C due to chemisorbed hydrogen increase with acidity of the support [23]. The change in catalytic properties are extensively discussed in [11,12]. The decrease in the width of the d-band with more positive charge on the support oxygens as illustrated in figure 12 will be explained in a forthcoming paper [24].

The AS functions as plotted in figure 10 and the fit results presented in table 5 for the Pt/Cl–Al_2O_3 catalysts show that for Pt particles dispersed onto the same support,

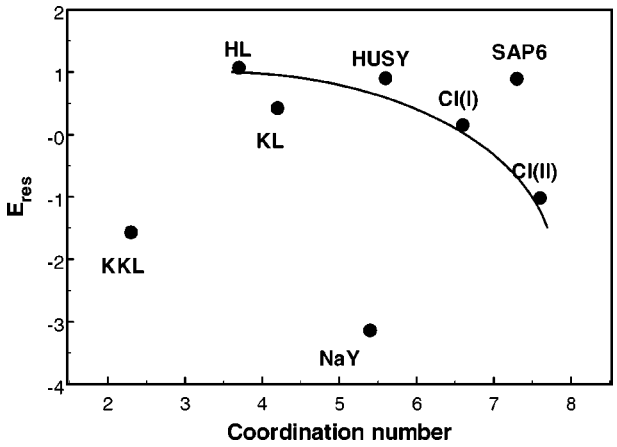

Figure 13. E_{res} plotted as a function of EXAFS coordination number. The solid line connects supports with comparable acidities, showing a particle size effect on E_{res}. The figure also dramatically illustrates the decrease in E_{res} with increasing alkalinity for the same particle size (e.g., at co-ordination number 5.5 for the Pt/Y and around 4 for the Pt/LTL samples).

E_{res} decreases with increasing particle size. The model as discussed above for the metal–support interaction indeed predicts that for larger metal particles the influence of the support will diminish since the fraction of metal atoms in direct contact with the support will decrease. In figure 13, the E_{res} values, as obtained for the catalysts studied in this paper, are plotted as a function of the Pt–Pt coordination number, which is proportional to the Pt particle size. Although some differences exist between the acidities and other properties of the different acidic supports, it is obvious that a general decrease in E_{res} can be observed with increasing particle size. Figure 13 also illustrates the dramatic reduction in E_{res}, with alkalinity (HL vs. KKL and HUSY vs. NaY), as discussed already in section 1. More data are needed to fully investigate the influence of the particle size on E_{res}. In particular the influence of increasing metallicity has to be studied. The results presented in figure 13 suggest that the onset of the metallicity occurs for particles with coordination numbers larger than 7.

6. Conclusion

Our previous work and the additional results presented here, demonstrate that the Pt–H resonance can be observed, and that its energy and spectral lineshape vary systematically with the alkalinity of the Pt cluster support and with cluster size. Generalisation to other metal atomic adsorbates and even molecular bonding has been shown. No measurement can more directly reflect the critical metal–adsorbate interaction, than observation of the bonding and antibonding orbitals constituting that interaction. The ability to watch the metal–adsorbate anti-bonding orbitals systematically vary with the alkalinity of the support provides a major new tool for understanding the fundamental mechanism of the metal–support interaction and its effects on the electronic structure and activity of the catalysts.

Acknowledgement

The authors would like to thank Dr. J.T. Miller (AMOCO Research Center, Naperville, USA) for encouragement, scientific discussions and the preparation of the Pt/LTL and Pt/Al_2O_3 samples. They are also thankful for the help and stimulating interest of the scientific staff of beamline BM29 of the ESRF (Grenoble, France), beamline 9.2 of the SRS (Daresbury, UK) and beamline X1.1 of the HASYLAB synchrotron (Hamburg, Germany).

References

[1] A.N. Mansour, J.W. Cook, Jr. and D.E. Sayers, J. Phys. Chem. 88 (1984) 2330.
[2] F.W. Lytle, R.B. Greegor, E.C. Marques, V.A. Biebesheimer, D.R. Sandstrom, J.A. Horsley, G.H. Via and J.H. Sinfelt, ACS Symp. Ser. 288 (1985) 280.
[3] M.G. Samant and M. Boudart, J. Phys. Chem. 95 (1991) 4070.
[4] M. Vaarkamp, J.T. Miller, F.S. Modica and D.C. Koningsberger, J. Catal. 163 (1996) 294.
[5] A.V. Soldatov, S. Della Longa and A. Bianconi, Solid State Commun. 8 (1993) 863.
[6] K. Asakura, T. Kubota, N. Ichikuni and Y. Iwasawa, Stud. Surf. Sci. Catal. 101 (1996) 911.
[7] S.N. Reifsnyder, M.M. Otten, D.E. Sayers and H.H. Lamb, J. Phys. Chem. B 101 (1997) 4972.
[8] B.I. Boyanov and T.I. Morrison, J. Phys. Chem. 100 (1996) 16318.
[9] D.E. Ramaker, B.L. Mojet, M.T. Garriga Oostenbrink, J.T. Miller and D.C. Koningsberger, J. Phys. Chem. Chem. Phys. 1 (1999) 2293.
[10] B.L. Mojet, D.E. Ramaker, J.T. Miller and D.C. Koningsberger, Catal. Lett. 62 (1999) 15.
[11] B.L. Mojet, J.T. Miller, D.E. Ramaker and D.C. Koningsberger, J. Catal. 186 (1999) 373.
[12] D.C. Koningsberger, J. de Graaf, B.L. Mojet, J.T. Miller and D.E. Ramaker, Appl. Catal. 191 (2000) 205.
[13] D.E. Ramaker, G.E. van Dorssen, B.L. Mojet and D.C. Koningsberger, Topics Catal. 10 (2000) 157.
[14] M. Vaarkamp, B.L. Mojet, F.S. Modica, J.T. Miller and D.C. Koningsberger, J. Phys. Chem. 99 (1995) 16067.
[15] J.W. Cook and D.E. Sayers, J. Appl. Phys. 52 (1981) 5024.
[16] B. Hammer and J.K. Nørskov, Nature 376 (1995) 238.
[17] W.E. O'Grady and D.E. Ramaker, Electrochim. Acta 44 (1998) 1283.
[18] L.F. Mattheiss and R.E. Dietz, Phys. Rev. B 22 (1980) 1663.
[19] M.K. Oudenhuijzen, J.H. Bitter and D.C. Koningsberger, J. Phys. Chem., submitted.
[20] J.H. Bitter, M.A. Cauqui, J.M. Gatica, S. Bernal, D.E. Ramaker and D.C. Koningsberger, J. Phys. Chem., submitted.
[21] A.J. Simoens, R.T.K. Baker, D.J. Dwyer, C.R.F. Lund and R.J. Madon, J. Catal. 86 (1984) 359.
[22] J.H.A. Martens, R. Prins, H. Zandbergen and D.C. Koningsberger, J. Phys. Chem. 92 (1988) 1903.
[23] P.V. Menacherry and G.L. Haller, J. Catal. 167 (1997) 425.
[24] D.E. Ramaker and D.C. Koningsberger, J. Catal., submitted.